Acta Cryst. (1997). **B53**, 373–380

Structural Studies of Rutile-Type Metal Dioxides

ADRIAN A. BOLZAN,[a] CELESTA FONG,[a] BRENDAN J. KENNEDY[a]* AND CHRISTOPHER J. HOWARD[b]

[a]*School of Chemistry, The University of Sydney, Sydney, NSW 2006, Australia, and* [b]*Australian Nuclear Science and Technology Organisation, Lucas Heights Research Laboratories, Private Mail Bag 1, Menai, NSW 2234, Australia. E-mail: kennedyb@alf.chem.su.oz.au*

(*Received 29 March 1995; accepted 27 January 1997*)

Abstract

The structures of the four metal dioxides GeO_2, SnO_2, RuO_2 and IrO_2 (germanium, tin, ruthenium and iridium dioxides, respectively) have been redetermined by Rietveld refinement from neutron diffraction powder data. The four dioxides all adopt the rutile-type structure, space group $P4_2/mnm$ (no. 136), with a = 4.4066 (1), 4.7374 (1), 4.4968 (2) and 4.5051 (3), c = 2.8619 (1), 3.1864 (1), 3.1049 (1) and 3.1586 (2) Å, and x = 0.3060 (1), 0.3056 (1), 0.3053 (1) and 0.3077 (3), respectively. These results are compared with those for other metal dioxides that adopt the rutile structure and trends in structural and thermal vibrations for a series of 11 metal dioxides which adopt the rutile-type structure are described.

1. Introduction

The structure and bonding in rutile-type AB_2 oxides and fluorides are of considerable theoretical importance (Burdett, 1985; Cox, 1992; Freeman & Catlow, 1992; Sorantin & Schwartz, 1992). The rutile structure is one of the simplest and most common structural types adopted by metal dioxides (Wells, 1984). At least ten metal dioxides have a polymorph with the rutile structure at room temperature, whereas two others, VO_2 (McWhan, Marezio, Remeika & Dernier, 1974) and NbO_2 (Bolzan, Fong, Kennedy & Howard, 1994), adopt the rutile structure at elevated temperatures. The structure of the third group V metal dioxide, TaO_2, remains controversial (Syono, Kikuchi, Goto & Fukora, 1983). In some cases the rutile structure is the most stable oxide, M = Ti, Ru, Ir, Sn, Pb, whereas for others the rutile is a metastable form produced under high temperature and pressure conditions, M = Rh, Si, Ge (Wells, 1984).

The rutile structure was first described by Vegard (1916) and has been studied, for various metals, consistently and with increasing accuracy over the ensuing 80 years (Baur, 1976, and references therein; Abrahams & Bernstein, 1971; Gonschorek, 1982; Burdett, Hughbanks, Miller, Richardson & Smith, 1987; Howard, Sabine & Dickson, 1991). Two parameters describe the rutile structure, namely the axial ratio c/a and the anion position parameter x. In addition, there are three independent thermal parameters for each anion and cation.

The rutile structure has edge-sharing octahedrally coordinated metal ions which form chains along the [001] direction. The chains are cross-linked by shared corners so that each chain is connected to four neighbouring chains. The MO_6 octahedra do not involve equal M—O bond distances, but rather are tetragonally distorted with both the apically compressed and apically elongated geometry being known, Fig. 1.† A feature of the rutile structure is that the O—O contacts within the MO_6 also are not equal, so the base of the octahedron is not square, the shared edge being shorter than the edge parallel to the c axis.

There are four areas of interest associated with the structure of rutile-type dioxides:

(i) Is there a systematic variation in the rectangular distortion of the base of the MO_6 octahedron?

(ii) What is the nature of the tetragonal distortion of the octahedra; is it elongated or compressed? This is determined by the values of c/a and x.

(iii) Are the metal–metal interactions significant? The dominant cation–cation interaction is in the c direction; M—M bonding results in a contraction in c and consequently a small c/a ratio or, in the extreme, a lowering of symmetry.

(iv) The anisotropic nature of the thermal parameters of the atoms, especially the anions. A variety of experimental methods and analysis models have been used to obtain the thermal motion data and there has been no attempt to date to explore systematic variations in them.

The structures of a number of the rutile-type dioxides have been accurately determined using high-resolution neutron and/or X-ray methods (Bolzan, Fong, Kennedy & Howard, 1994; Howard, Sabine & Dickson, 1991; Baur, 1976; Burdett, Miller, Richardson & Smith, 1988;

† The M at (0, 0, 0) is coordinated to six O atoms. The O atoms at $\pm(x, x, 0)$ are referred to as the apical O atoms and those at $\pm(\frac{1}{2} - x, x - \frac{1}{2}, \pm\frac{1}{2})$ as equatorial. The apical and equatorial M—O bond distances are generally of different lengths, this being referred to as the tetragonal distortion. The rectangle formed by the four equatorial O atoms is referred to as the base of the octahedron.

Bolzan, Fong, Kennedy & Howard, 1993; D'Antonio & Santoro, 1980). However, prior to our commencing this work the oxygen position parameter and thermal vibrations for most of the heavier metal oxides, M = Nb, Ru, Ir, Sn, were not well described. The Rietveld (1969) method of profile analysis of neutron diffraction powder data is known to yield accurate structural and thermal parameters for metal oxides (Young, 1993). Although methods for the preparation of single crystals of all the rutile-type dioxides, except RhO_2 (Rogers, Shannon, Sleight & Gillson, 1969), are known, it was considered that powder neutron diffraction would provide precise and accurate crystallographic parameters for the heavier rutiles.

The aim in this paper is to present the results from the Rietveld analysis of neutron diffraction powder patterns of IrO_2, SnO_2, RuO_2 and GeO_2, and to compare the results obtained for these materials with those for other metal dioxides. For the first time a large number of rutile-like dioxides has been studied and analysed under identical conditions, allowing detailed discussion of periodic trends in the various crystallographic parameters.

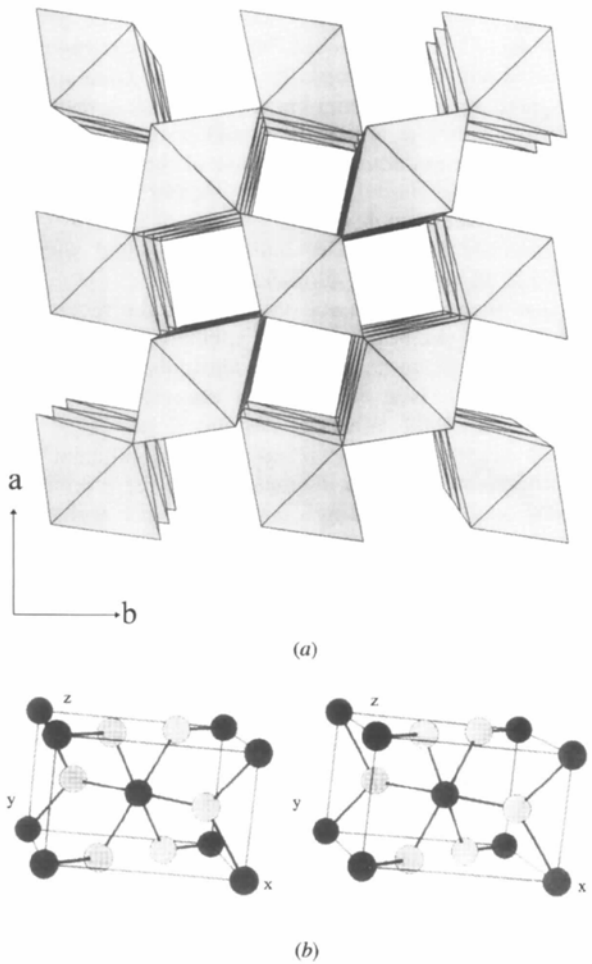

Fig. 1. (*a*) The rutile structure viewed along the *c* axis and (*b*) as a steroview, in which the *M* atoms are represented by the darker spheres.

2. Experimental and data analysis

Tetragonal GeO_2 was prepared by the hydrothermal conversion of the hexagonal phase using the procedure described by Brauer (1962). GeO_2 (Aldrich) was heated at 620 K for 48 h at a pressure of approximately 14 MPa produced by super-heated water.

IrO_2 was prepared by the thermal decomposition of $IrCl_3$ (Aldrich) at 1170 K for 1 h under flowing O_2.

RuO_2 was prepared by the dehydration of $RuO_2.xH_2O$ (Aldrich), followed by thermal annealing at 1170 K under flowing O_2.

SnO_2 was obtained from Aldrich and examined as received.

Neutron diffraction powder patterns were recorded using the high-resolution powder diffractometer (HRPD) on the Australian Nuclear Science and Technology Organisation's (ANSTO) HIFAR reactor (Howard, Ball, Davis & Elcombe, 1983). The samples were contained in thin-walled vanadium cans, which were rotated throughout the measurements to reduce the effects on intensities of preferred orientation. Intensities were recorded, using eight detectors, in 0.05 steps.* All structural refinements were performed using a version of Hill & Howard's (1986) program *LHPM*, modified for use on a personal computer. A Voigt function was used to model the shape of the peaks. The width of the Gaussian component was taken to vary in accordance with the expression due to Caglioti, Paoletti & Ricci (1958), modified as described by Elcombe & Howard (1988) to allow for anisotropic strain broadening. The data were corrected for absorption as described by Hewat (1979). The width of the Lorentzian component was coded to vary with $\sec\theta$ in an attempt to model particle size broadening. The scattering lengths used were: Ru, 0.721; Sn, 0.6228; Ir, 1.0600; Ge, 0.8193; O, 0.5805 fm. Further details are given in Table 1.

3. Results

3.1. *GeO_2*

The starting values for the lattice parameter and position parameter were taken from Baur & Khan (1971). The standard Rietveld refinement converged rapidly, R_{wp} = 0.0511 and R_B = 0.0147, however, the fit showed small index-dependent discrepancies between the observed and calculated peak widths in the range $100 < 2\theta < 125°$ with the $(00l)$-type lines being narrow.

* The numbered intensity of each measured point on the profile has been deposited with the IUCr (Reference: BR0044). Copies may be obtained through The Managing Editor, International Union of Crystallography, 5 Abbey Square, Chester CH1 2HU, England.

Table 1. *Details of data collection and refinement*

	GeO_2	RuO_2	SnO_2	IrO_2
Neutron wavelength (Å)*	1.372	1.377	1.377	1.372
2θ Scan range (°)	20–154	18–158	18–158	15–145
2θ Scan step size (°)	0.05	0.05	0.05	0.05
Maximum step intensity†	2×10^4	10^4	10^4	2×10^4
No. of reflections	56	65	74	62
No. of refined parameters‡	21	23	20	21
R_{wp}	0.0408	0.0499	0.0507	0.0776
R_{exp}	0.0285	0.0393	0.0423	0.0603
R_{Bragg}	0.0091	0.0127	0.0133	0.0230
a (Å)	4.40656(5)	4.4968(2)	4.73735(9)	4.5051(3)
c (Å)	2.86186(3)	3.1049(1)	3.18640(7)	3.1586(2)
x	0.30604(6)	0.3053(1)	0.30562(9)	0.3077(3)
Anisotropic displacement parameters ($Å^2 \times 10^{-3}$)				
M				
U^{11}	3.3(1)	3.9(2)	4.4(3)	11.0(5)
U^{12}	0.0(2)	−0.7(2)	−0.4(2)	−0.4(4)
U^{33}	2.3(2)	4.4(5)	3.1(4)	6.4(8)
O				
U^{11}	3.9(6)	6.3(3)	6.6(2)	12.1(6)
U^{12}	−0.9(1)	−2.1(2)	−1.6(2)	−2.9(4)
U^{33}	3.1(2)	7.0(4)	5.5(4)	7.0(9)

* The wavelength was defined from the (117) reflection from a Ge monochromator. † Pre-set aggregate in eight detectors. § R factors as defined by Rietveld (1969). ‡ A full listing of all refined parameters is available as supplementary data.

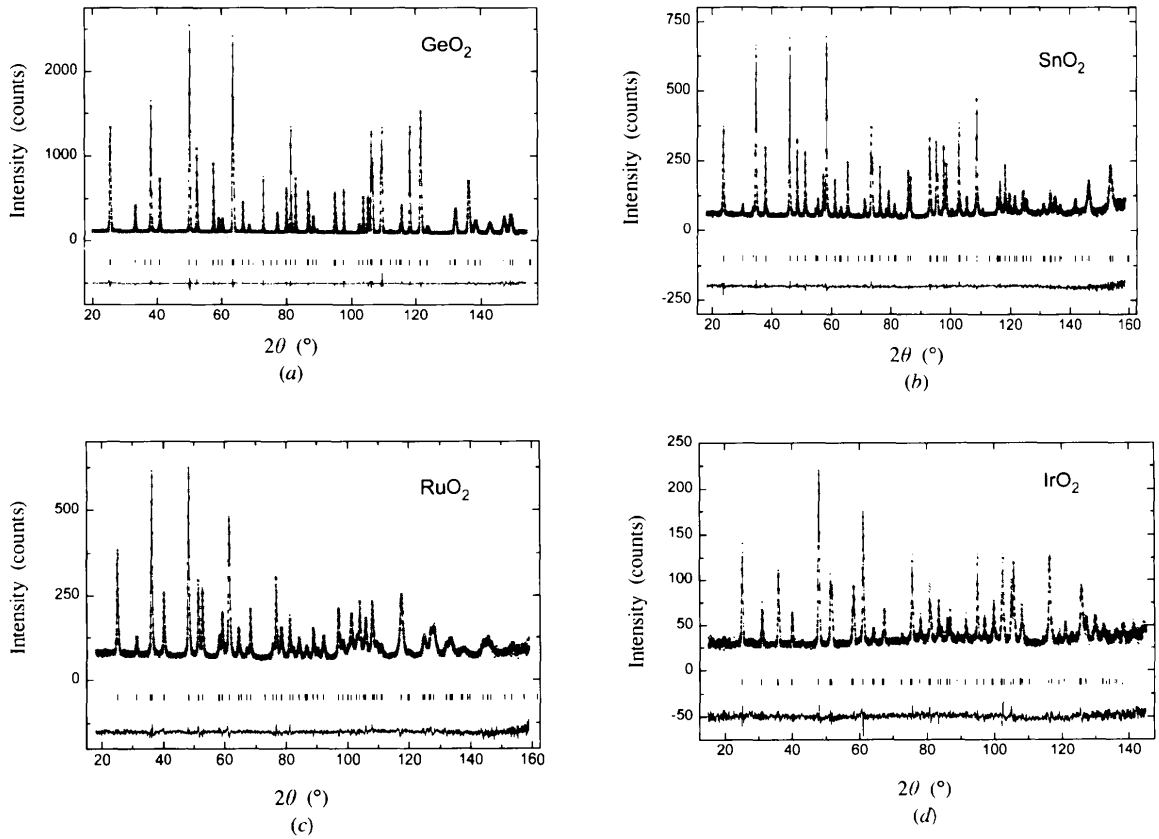

Fig. 2. Neutron powder patterns for (*a*) GeO_2, (*b*) SnO_2, (*c*) RuO_2 and (*d*) IrO_2. In each case the difference between the observed (x) and calculated (solid line) patterns is shown in the lower trace. All allowed Bragg reflections are shown by vertical lines.

Table 2. *Structural data for some metal dioxides adopting the rutile structure*

		TiO_2	VO_2	CrO_2	MnO_2	NbO_2	
Metal ionic radii (Å)		0.68	0.63	0.62	0.60	0.74	
Lattic parameters (Å)							
	a	4.5937 (1)	4.5546 (3)	4.4219 (3)	4.3980 (1)	4.8464 (1)	
	c	2.9587 (1)	2.8514 (2)	2.9166 (4)	2.8726 (1)	3.0316 (1)	
c/a ratio		0.6441 (3)	0.6260 (1)	0.6596 (1)	0.65316 (3)	0.62554 (2)	
Oxygen position	x	0.30478 (6)	0.3001 (2)	0.3024 (8)	0.3046 (1)	0.2925 (2)	
Anisotropic displacement parameters ($Å^2 \times 10^{-3}$)							
Metal	U^{33}	4.6 (5)	9.6 (3)	1.7 (4)	2.3 (8)	33.8 (6)	
	$U^{11} - U^{12}$	7.2 (4)	12.3 (4)	4.2 (5)	3.2 (4)	22 (1)	
	$U^{11} + U^{12}$	6.4 (4)	10.0 (4)	5.0 (5)	5.6 (4)	20 (1)	
Oxygen	U^{33}	3.5 (2)	6.2 (1)	4.4 (2)	4.2 (4)	26.9 (9)	
	$U^{11} - U^{12}$	7.2 (2)	10.4 (4)	8.1 (3)	11 (1)	41 (1)	
	$U^{11} + U^{12}$	3.2 (2)	6.7 (4)	4.1 (3)	4.1 (5)	21 (1)	
Interatomic separations (Å)							
Equatorial M—O		1.949 (1)	1.921 (1)	1.911 (1)	1.882 (2)	2.079 (3)	
Axial M—O		1.980 (1)	1.933 (1)	1.891 (1)	1.894 (1)	2.005 (1)	
O—O(O_s)		2.536 (2)	2.575 (1)	2.471 (3)	2.431 (1)	2.844 (2)	
M—M		3.569 (1)	3.522 (1)	3.450 (1)	3.426 (9)	3.747 (8)	
O_s/O_u*		0.855	0.905	0.849	0.843	0.939	
Reference		(*a*)	(*b*)	(*c*)	(*d*)	(*e*)	
		RuO_2	IrO_2	SiO_2	GeO_2	SnO_2	PbO_2
Metal ionic radii (Å)		0.67	0.68	0.42	0.53	0.71	0.84
Lattice parameters (Å)							
	a	4.4968 (2)	4.5051 (3)	4.1773 (3)	4.4066 (1)	4.7374 (1)	4.9577 (1)
	c	3.1049 (1)	3.1586 (2)	2.6655 (1)	2.8619 (1)	3.1864 (1)	3.3879 (8)
c/a ratio		0.6905 (1)	0.7011 (2)	0.6381 (1)	0.6494 (3)	0.6726 (1)	0.6834 (2)
Oxygen position	x	0.3053 (1)	0.3077 (3)	0.30608 (6)	0.30604 (6)	0.3056 (1)	0.3072 (1)
Anisotropic displacement parameters ($Å^2 \times 10^{-3}$)							
Metal	U^{33}	4.4 (5)	6.4 (8)	1.8 (1)	2.3 (2)	3.1 (4)	5.0 (4)
	$U^{11} - U^{12}$	4.6 (4)	11.4 (9)	2.2 (1)	3.3 (3)	4.8 (5)	9.6 (5)
	$U^{11} + U^{12}$	3.2 (4)	10.6 (9)	2.5 (1)	3.3 (3)	4.0 (5)	7.6 (5)
Oxygen	U^{33}	7.0 (4)	7.0 (9)	2.3 (10)	3.1 (2)	5.5 (4)	7.2 (4)
	$U^{11} - U^{12}$	8.4 (5)	15.0 (10)	4.0 (1)	4.8 (7)	8.3 (4)	21.0 (5)
	$U^{11} + U^{12}$	4.1 (5)	9.2 (10)	2.1 (1)	3.0 (7)	5.0 (4)	7.0 (5)
Interatomic separations (Å)							
Equatorial M—O		1.985 (2)	1.998 (2)	1.757 (2)	1.874 (4)	2.058 (2)	2.167 (2)
Axial M—O		1.941 (1)	1.958 (1)	1.808 (4)	1.906 (7)	2.047 (1)	2.154 (1)
O—O(O_s)		2.476 (1)	2.451 (3)	2.291 (1)	2.4170 (1)	2.605 (1)	2.704 (1)
M—M		3.538 (1)	3.553 (4)	3.241 (1)	3.429 (9)	3.709 (1)	3.893 (1)
O_s/O_u*		0.799	0.777	0.860	0.844	0.816	0.798
Reference		(*f*)	(*f*)	(*g*)	(*f*)	(*f*)	(*h*)

* This shows the ratio of the shared-edge O—O distance (O_s) to the O—O distance along the unshared edge ($O_u = c$). (*a*) Howard, Sabine & Dickson (1991); (*b*) McWhan, Marezio, Remeika & Dernier (1974); (*c*) Burdett, Miller, Richardson & Smith (1988); (*d*) Bolzan, Fong, Kennedy & Howard (1993); (*e*) Bolzan, Fong, Kennedy & Howard (1994); (*f*) This work; (*h*) Hill, Newton & Gibbs (1983); (*h*) Kisi, unpublished work.

The fit was considerably improved (Fig. 2*a*) by assuming anisotropic broadening based on cell-to-cell variation in the a parameter, akin to the α-PbO case discussed by Elcombe & Howard (1988), but replacing the minus sign in the numerator with a plus sign. The refined value of $\Delta a/a_o$ was 0.2%. Table 1 lists the details of the data collection and refinement and the final results are given in Table 2. The nature of the anisotropic broadening has been confirmed by a high-resolution X-ray diffraction study on the Australian diffractometer at the Photon Factory, Tsukuba, Japan (Sabine, Kennedy, Garrett, Foran & Cookson, 1995).

3.2. *SnO_2*

Refinement of the unit-cell dimensions, oxygen position parameter x and anisotropic thermal parameters for SnO_2 led directly to a good fit (Fig. 2*b*). The final parameters are given in Table 1.

3.3. *RuO_2*

As in the case of GeO_2, the standard refinement gave a fit showing some discrepancies between observed and calculated peak widths. Refinement using the same model for anisotropic broadening as for GeO_2 led to an

improved fit, with $\Delta a/a_o$ = 0.5% (Fig. 2*c*). Refinement of the occupancies showed the material to be non-stoichiometric, $Ru_{0.95}O_2$. The corresponding parameters are listed in Table 1.

3.4. IrO_2

As a consequence of the high neutron absorption cross section of iridium, the signal-to-noise in the pattern of this complex is relatively poor (Fig. 2*d*). Nevertheless, a well resolved diffraction pattern was obtained which, after correction for absorption (μR = 1.50), was fitted to give the parameters listed in Table 1.

4. Discussion

The data for 11 rutile-type dioxides are summarized in Table 2. With the exception of SiO_2 (Hill, Newton & Gibbs 1983) and VO_2 (McWhan, Marezio, Remeika & Dernier 1974), the data have been obtained from powder neutron diffraction. Of these nine structural determinations, all but that of CrO_2 (Burdett, Miller, Richardson & Smith 1988) are based on data recorded using the HRPD at ANSTO and analysed using the program *LHPM*. It is apparent from Table 2 that both 2 long + 4 short (2L + 4S) and 4 long + 2 short (4L + 2S) geometries are found in the rutile-type dioxides. Fig. 3 shows a plot of x *versus* c/a, which is an updated version of that given by Baur (1976). The solid line corresponds to a regular octahedral geometry. Compounds above the line have a (2L + 4S) geometry and those below it a (4L + 2S) geometry. It should be noted that the results for SnO_2 and PbO_2, which were shown above the line in Baur's (1976) figure, are now seen below the line, corresponding to a (4L + 2S) geometry. One feature of Fig. 3 is that, except for Nb, V and to a lesser extent Cr, the oxygen position parameter x is essentially independent of the c/a ratio, with an average value of x = 0.306 (1).

The low values of x observed for NbO_2, VO_2 and CrO_2 can be rationalized by noting that all these compounds have atypical electronic properties. For both NbO_2 and VO_2, to obtain the rutile phase it is necessary to record the diffraction pattern at elevated temperatures, but we do not believe that this is the reason for the lower observed values of x. There is indeed evidence that the x position in rutiles is essentially independent of temperature – for TiO_2 Sugiyama & Takeuchi (1991) found x to be independent of temperature up to 1970 K and for SiO_2 it remains constant up to 673 K (Endo *et al.*, 1986), which is just below the decomposition temperature. Thus, it appears that electronic interactions associated with the low c/a values observed for the two oxides VO_2 and NbO_2 are the most probable origin of the lower than usual x value (Bolzan, Fong, Kennedy & Howard, 1994). CrO_2 is unique in this series of oxides in that it is the only ferromagnet.

The lattice parameters show large differences between the various metal oxides, there being striking correlation between the ionic radii of the cation and the lattice constants a and c (Fig. 4). For the group 14 metals Si, Ge, Sn and Pb there is a precise linear relationship. As can be seen from Fig. 5, the M—O distances in the group 14 oxides also display, as expected, a precise linear increase with the metal ionic radii. In contrast for the transition metals the M—O distances fall below the line fitting the group 14 data. The difference between the two series is, of course, that each of the nine transition metals has unfilled d orbitals available for bonding, whereas the group 14 oxides do not.

Starting with Pauling (1928) there have been numerous attempts to rationalize the rutile structure (Freeman & Catlow 1992; Sorantin & Schwartz, 1992; Burdett,

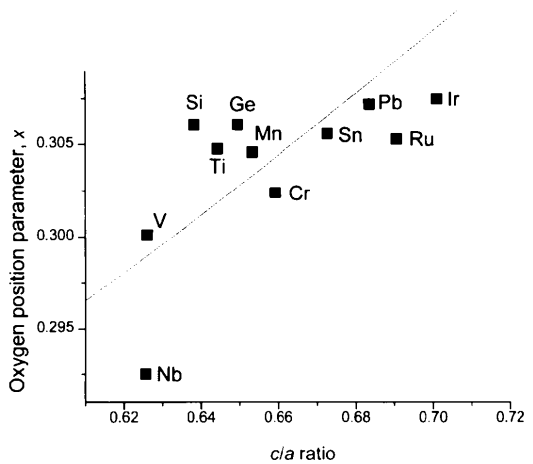

Fig. 3. The oxygen positional parameter (x) *versus* the ratio of the lattice constants (c/a). The solid line is where the axial and equatorial M—O bond distances are equal. For compounds above the line the coordination octahedron is apically elongated, *i.e.* 2L + 4S.

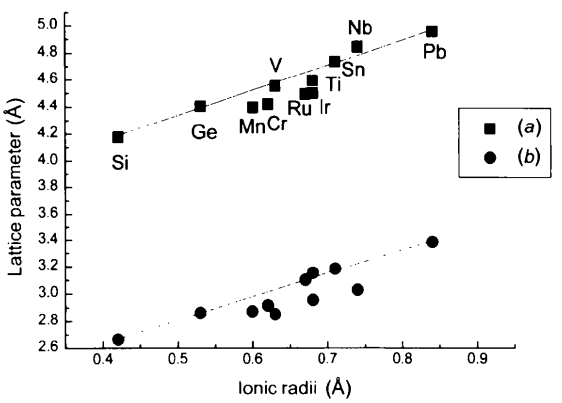

Fig. 4. Plot of the lattice constants a and c *versus* metal ionic radius for the 11 rutile-type dioxides. The solid line is a linear fit for the four group 14 dioxides.

1985; Baur, 1976; Burdett, Miller, Richardson & Smith, 1988). Without reviewing the findings in detail here, a key point to emerge from these studies is that bonding in TiO_2 is not purely ionic, but rather that the Ti—O bonds are partially covalent in character. The most probable interaction involves π back-donation from the oxygen π orbital perpendicular to the Ti_3 plane of the OTi_3 groups; this type of interaction must be absent in the group 14 metals. This effect appears to result in a contraction of the *M*—O distance in the transition metal rutiles, which is greater than the average for transition metal oxides from which ionic radii have been determined (Shannon, 1976).

The observation that the group 14 metals do not all display the same type of tetragonal distortions, Si and Ge being (4S + 2L) and Sn and Pb being (4L + 2S), suggests that even for the group 14 metals a simple ionic model is not appropriate.

Further evidence of the inappropriateness of the simple ionic model is found by considering the shortening of the O—O distance along the shared edge, O_s, relative to the unshared O—O distance along *c*, $O_u = c$. Electrostatic energy calculations based on a point charge model (Argyriou & Howard, 1992) indicate that the ratio of O_s/O_u should be small ($\sim$ 0.5), but it is increased by O—O repulsions. Only if the cell is large do the O atoms have sufficient space to achieve a minimal value of O_s/O_u. For the four group 14 metal oxides the ratio O_s/O_u decreases down the group, Si, Ge, Sn, Pb, *i.e.* as the cell volume increases, due to the diminishing importance of the non-bonded O—O repulsions in larger volume cells.

Considering the transition metal oxides RuO_2 and IrO_2 the O_s/O_u ratio is smaller than would be expected for group 14 metal oxides of similar cell size. Conversely, for TiO_2, CrO_2 and MnO_2 the O_s/O_u ratio is slightly larger than would be expected if only electrostatics and size were considered. It appears that not only does the presence of unfilled *d* orbitals result in changes to the *M*—O bonding (Rogers, Shannon, Sleight & Gillson, 1969), but also they appear to alter the precise nature of the various O—O interactions, presumably by changing the electron density on the oxygen groups.

The base of the MO_6 octahedron in VO_2 and NbO_2 is considerably more regular than for the other rutiles, $O_s/O_u > 0.9$. For these complexes, which adopt the regular rutile structure only at high temperatures, the unshared O—O distance (= *c*) is unusually small, presumably as a consequence of the strong *M*—*M* interaction in these complexes.

In developing a model to fully explain the precise structural trends in the rutile-type dioxides it appears that at least four effects need to be considered, namely electrostatic interactions, cell volume, *d*-orbital occupancy and metal–metal interactions.

The thermal vibration parameters of the O atoms in rutile-type dioxides increase with increasing unit-cell volume (the data for NbO_2 were obtained at high temperatures and should not be included in this trend) and are strongly anisotropic (Table 2). The principal axes of vibration lie along the [001] direction, which is parallel to the *c* axis, and the [110] and [1$\bar{1}$0] directions; the mean-square vibrational amplitudes for these directions are U^{33}, $U^{11} + U^{12}$ and $U^{11} - U^{12}$, respectively (Howard, Sabine & Dickson 1991; Bolzan, Fong, Kennedy & Howard, 1993). The vibrations in the *ab* plane, with the metal atoms at $z = 0$, are illustrated in Fig. 6. It can be seen that the O—*M*—O moieties lie along [110], so that the mean-square amplitudes $U^{11} + U^{12}$, in the [110] direction, and $U^{11} - U^{12}$, in the [1$\bar{1}$0] direction, refer to vibrations along and perpendicular to the O—*M*—O moieties, respectively. This last vibration is the largest in all the rutile-type dioxides.

There are two complementary arguments to explain the anisotropy in the oxygen thermal displacements. The first, proposed by Pauling (1980), is a bond-stretching

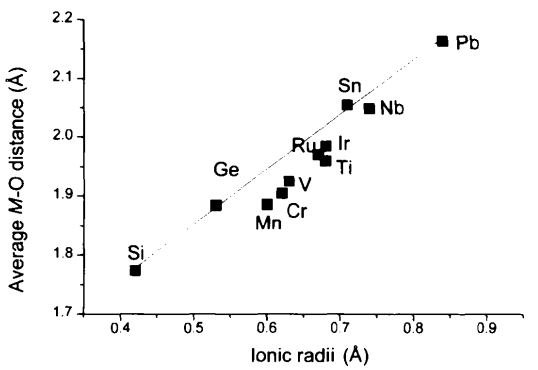

Fig. 5. Plot of the average metal–oxygen bond distance *versus* the metal ionic radius. The solid line is a linear fit for the four group 14 dioxides.

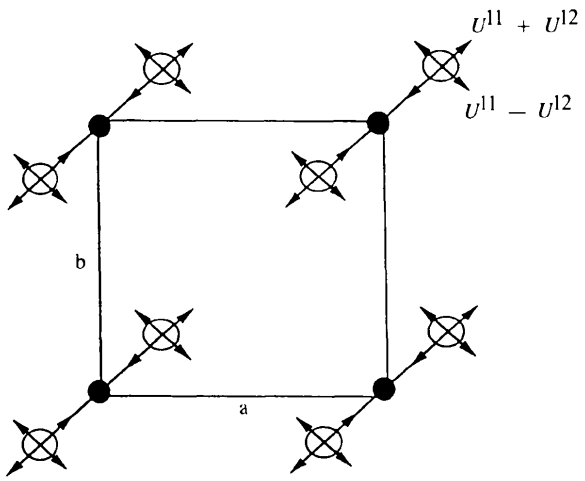

Fig. 6. Directions of the oxygen principal mean square vibrations in the *ab* plane. The metal atoms are represented by the darker spheres.

argument and the second, proposed by Howard, Sabine & Dickson (1991), is based on the stereochemistry of the O atoms. The O atoms form three bonds in a plane. All vibrations within the plane will involve a shortening of one of the strong *M*—O bonds; only the movement of the O atom perpendicular to the plane of the OM_3 unit is free of any first-order bond compression. Examination of the rutile structure, Fig. 7, shows that the closest contact to an O atom perpendicular to the OM_3 unit is at $a/2^{1/2}$, whereas the closest contacts along the other principal vibration axes are at $2^{1/2}xa$ (one of the *M*—O bonds) and *c*. Thus, the $U^{11} - U^{12}$ displacement is expected to be larger since it involves movement into a large void without compression of any of the *M*—O bonds. The other two principal vibrations $U^{11} + U^{12}$ and U^{33} will involve both bond compression and movement into more crowded parts of the structure.

In general, the thermal motions of the metal atoms are smaller than those of the oxygens, the two exceptions being Ti and V. Whereas the metal thermal parameters all indicate anisotropic motion, the anisotropy is less than observed for the oxygen groups. This is in accordance with the approximately octahedral geometry of the metal.

In general, the metal displacements in the *ab* plane ($U^{11} \pm U^{22}$) are larger than the *c*-axis displacement (U^{33}), irrespective of the nature of the tetragonal distortion. This indicates that the motion of the metal is not solely controlled by minimization of bond-contraction effects, but rather that second-order contacts also contribute to this effect.

5. Conclusions

In the introduction to this work four questions were posed. These can now be answered as follows:

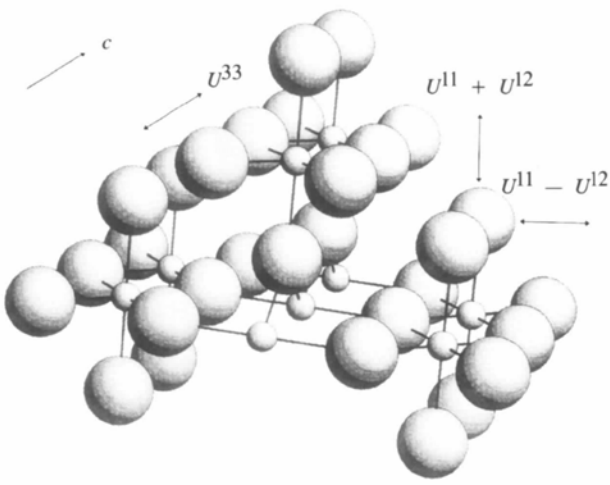

Fig. 7. A three-dimensional view of part of the rutile lattice showing the principal axes of vibration. Note that the U^{33} vibration is along the *c* axis. The metal atoms are represented by the smaller spheres.

(i) It is clear that the rectangular distortion of the base of the MO_6 octahedron is dependent on the cell volume, which in turn is controlled by the ionic radius of the metal. This relationship between the rectangular distortion and cell volume is not a simple one, but is modified by *M*—*M* interactions.

(ii) The unique oxygen positional parameter is essentially constant for the rutile-type dioxides unless unusual electronic factors are important. The tetragonal distortion of the MO_6 octahedron is weakly dependent on the *c*/*a* ratio of the metal; for larger *c*/*a* ratios an apically compressed (4L + 2S) arrangement is favoured.

(iii) Metal–metal interactions are significant. This is especially true for the d^1 compounds VO_2 and NbO_2. For the transition metal dioxides the use of low-energy *d* orbitals in π bonding with the O atoms is significant.

(iv) The magnitude of the thermal vibrations of the atoms are correlated with the size of the cell. For the anions in particular the vibrations are anisotropic, displacements into voids and/or avoiding bond compression being favoured.

It is hoped that establishing precise and accurate structural parameters for a wide range of rutile-type metal dioxides will stimulate further attempts to model these structures fully.

The support of the Australian Institute of Nuclear Science and Engineering for this work is gratefully acknowledged. We thank Dr Erich Kisi for making available to us his unpublished results from β-PbO_2.

References

Abrahams, S. C. & Bernstein, J. L. (1971). *J. Chem. Phys.* **55**, 3206–3211.

Argyriou, D. N & Howard, C. J. (1992). *Aust. J. Phys.* **45**, 239–252.

Baur, W. H. (1976). *Acta Cryst.* B**32**, 2200–2204.

Baur, W. H. & Khan, A. A. (1971). *Acta Cryst.* B**27**, 2133–2139.

Bolzan, A. A., Fong, C., Kennedy, B. J. & Howard, C. J. (1993). *Aust. J. Chem.* **46**, 939–944.

Bolzan, A. A., Fong, C., Kennedy, B. J. & Howard C. J. (1994). *J. Solid State Chem.* **113**, 9–14.

Burdett, J. K. (1985). *Inorg. Chem.* **24**, 2244–2253.

Burdett, J. K., Hughbanks, T., Miller, G. J., Richardson, J. W. & Smith, J. V. (1987). *J. Am. Chem. Soc.* **109**, 3639–3646.

Burdett, J. K., Miller, G. J., Richardson, J. W. & Smith, J. V. (1988). *J. Am. Chem. Soc.* **110**, 8064–8071.

Brauer, G. (1962). *Handbook of Preparative Inorganic Chemistry*. Academic Press, New York.

Caglioti, G., Paoletti, A. & Ricci, F. P. (1958). *Nucl. Instrum.* **3**, 223–228.

Cox, P. A. (1992). *Transition Metal Oxides*. Oxford: Clarendon Press.

D'Antonio, P. & Santoro, A. (1980). *Acta Cryst.* B**36**, 2394–2397.

Elcombe, M. M. & Howard C. J. (1988). *Mater. Sci. Forum*, **27/28**, 71–76.

Endo, S., Akai, T., Akahama, Y., Wakatsuki, M., Nakamura, T., Tomii, Y., Koto, K., Ito, Y. & Tokonami, M. (1986). *Phys. Chem. Miner.* **13**, 146–151.

Freeman, C. M. & Catlow, C. R. A. (1992). *J. Chem. Soc. Chem. Commun.* pp. 89–91.

Gonschorek, W. (1982). *Z. Kristallogr.* **160**, 187–203.

Hewat, A. W. (1979). *Acta Cryst.* A**35**, 248.

Hill, R. J. & Howard, C. J. (1986). Australian Atomic Energy Commission Report No. AAEC/M112, AAEC (now ANSTO). Lucas Heights Research Laboratories, New South Wales, Australia.

Hill, R. J., Newton, M. D. & Gibbs, G. V. (1983). *J. Solid State Chem.* **47**, 185–200.

Howard, C. J., Ball., C. J., Davis, R. L. & Elcombe, M. M. (1983). *Aust. J. Phys.* **36**, 507–518.

Howard, C. J., Sabine, T. M. & Dickson, F. (1991). *Acta Cryst.* B**47**, 462–468.

McWhan, D. B., Marezio, M., Remeika, J. P. & Dernier, P. D. (1974). *Phys. Rev. B*, **10**, 490–495.

Pauling, L. (1928). *Z. Kristallogr.* **67**, 377–404.

Pauling, L. (1980). *Acta Cryst.* B**36**, 761–762.

Rietveld, H. M. (1969). *J. Appl. Cryst.* **2**, 65–71.

Rogers, D. B., Shannon, R. D., Sleight, A. W. & Gillson, J. L. (1969). *Inorg. Chem.* **8**, 841–849.

Sabine, T. M., Kennedy, B. J., Garrett, R., Foran, G. & Cookson D. (1995). *J. Appl. Cryst.* **28**, 513–517.

Shannon, R. D. (1976). *Acta Cryst.* A**32**, 751–767.

Sorantin, P. I. & Schwartz, K. (1992). *Inorg. Chem.* **31**, 567–576.

Sugiyama, K. & Takeuchi, Y. (1991). *Z. Kristallogr.* **197**, 307–313.

Syono, Y., Kikuchi, M., Goto, T. & Fukora, K. (1983). *J. Solid State Chem.* **50**, 133.

Vegard, L. (1916). *Philos. Mag.* **32**, 505–518.

Wells, A. F. (1984). *Structural Inorganic Chemistry*. Oxford: Clarendon Press.

Young, R. A. (1993). Editor. *The Rietveld Method*. Oxford University Press.